




Article

Alkali-Free Zn–Al Layered Double Hydroxide Catalysts for Triglyceride Transesterification

Nazrizawati A. Tajuddin ^{1,2}, Jinesh C. Manayil ¹, Mark A. Isaacs ³ , Christopher M.A. Parlett ⁴ , Adam F. Lee ⁵  and Karen Wilson ^{5,*}

¹ European Bioenergy Research Institute (EBRI), Aston University, Birmingham B4 7ET, UK; nazriza@uitm.edu.my (N.A.T.); j.manayil@aston.ac.uk (J.C.M.)

² Department of Chemistry, Perak Campus, University of Technology MARA, Tapah Road, Tapah Branch 35400, Perak, Malaysia

³ Department of Chemistry, University College London, London WC1H 0AJ, UK; mark.isaacs@ucl.ac.uk

⁴ School of Chemical Engineering & Analytical Science, The University of Manchester, The Mill, Sackville Street, Manchester M13 9PL, UK; christopher.parlett@manchester.ac.uk

⁵ Applied Chemistry and Environmental Sciences, School of Science, RMIT University, 124 La Trobe Street, Melbourne, VIC 3000, Australia; adam.lee2@rmit.edu.au

* Correspondence: karen.wilson2@rmit.edu.au; Tel.: +61-(03)-99252122

Received: 11 November 2018; Accepted: 13 December 2018; Published: 18 December 2018

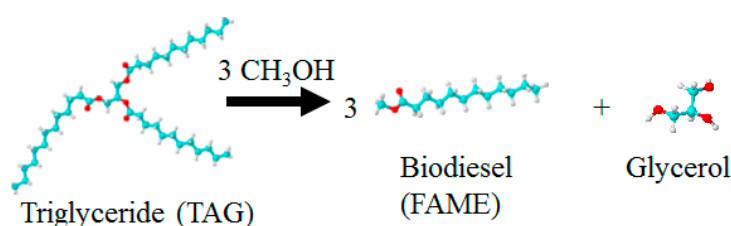


Abstract: Zn–Al layered double hydroxides (LDHs) of general formula $[Zn^{2+}_{(1-x)}Al^{3+}_x(OH)_2]^{x+}(CO_3^{2-})_{x/2} \cdot yH_2O$ are promising solid base catalysts for the transesterification of lipids to biofuels. However, conventional synthetic routes employ alkali hydroxide/carbonate precipitants which may contaminate the final LDH catalyst and biofuel. The use of $(NH_3)_2CO_3$ and NH_3OH as precipitants affords alkali-free Zn–Al-LDHs spanning a wide composition range. The hydrothermal reconstruction of calcined Zn–Al-LDHs offers superior solid basicity and catalytic activity for the transesterification of C_4 – C_{18} triglycerides with methanol, compared with cold liquid phase or vapour phase reconstruction. Hydrothermally activated $Zn_{3.3}$ –Al-LDH was stable towards leaching during transesterification.

Keywords: biodiesel; layered double hydroxides; transesterification; solid base; triglycerides

1. Introduction

Biodiesel is an attractive renewable liquid transportation fuel when derived from non-edible plant [1] or algal oils [2], animal fats [3], or waste cooking oil [4], and can be used as a standalone fuel or blended with petroleum-derived diesel [5–7]. Commercial routes to biodiesel, which comprises fatty acid methyl esters (FAMES), employ soluble alkali methoxides to transesterify C_{14} – C_{20} triacylglyceride (TAG) components of lipids with light alcohols (Scheme 1), but are environmentally unsustainable due to the large quantity of waste water generated during biodiesel isolation and purification [8,9].



Scheme 1. Transesterification of triglyceride to biodiesel and glycerol by-product.

Solid base catalysts are an attractive alternative to alkali methoxides [10–14], offering facile product separation and hence eliminating quenching steps, thereby reducing waste water formation and enabling process intensification through continuous operation [15].

Layered double hydroxides (LDHs) of general formula $[M^{2+}_{(1-x)}M^{3+}_x(OH)_2][A^{n-}]_{x/n} \cdot yH_2O$ (where x spans 0.2–0.4) are a class of inorganic materials comprising lamellar brucite-like layers containing mixed M^{2+} and M^{3+} cations, separated by an interlayer of charged anions (A^{n-}) [16,17]. The ability to vary the $M^{2+}:M^{3+}$ ratio and hence tune their physicochemical properties, renders LDHs valuable heterogeneous catalysts [18–21]. Most synthetic LDHs are prepared by the co-precipitation of M^{2+} and M^{3+} salts under basic conditions, which results in the entrainment of residual alkali [22–24]. In the context of biodiesel synthesis, entrained Na^+ and K^+ are highly soluble in light alcohols, and their leaching is associated with homogeneous catalysis, in addition to the saponification and emulsification of fatty acids impurities in the oil feedstock.

To date, Mg–Al-LDHs (usually termed hydrotalcites) have proven highly active and tunable catalysts for triglyceride transesterification, with alkali-free co-precipitation from nitrate precursors using NH_4CO_3 and NH_3OH as pH regulators reported [25,26]. Sol-gel routes to Mg–Al-LDHs from expensive Al and Mg methoxide precursors are also known [27]. Urea hydrolysis offers an alternative route to LDHs [28], such as $[Zn_{0.67}Al_{0.33}(OH)_2](CO_3)_{0.165} \cdot 0.5H_2O$, but requires post-modification with Na_2CO_3 to produce a pure LDH phase [22,29], which again risks complications from entrained alkali. It is, therefore, surprising that the use of NH_4CO_3 and NH_3OH precipitants has not been extended to other $M^{2+}:Al^{3+}$ combinations utilised in LDH synthesis [25].

Biodiesel production over spinel zinc aluminate ($ZnAl_2O_4$) prepared by calcination of Zn–Al-LDHs [30,31] has attracted significant attention and was commercialised as a continuous process by IFP [32]. Recent studies suggest that alkali-precipitated Zn–Al-LDHs dehydrated by low temperature calcination at 200 °C (insufficient to form crystalline spinels) exhibit superior performance for triglyceride transesterification, giving a stable 76% FAME yield from soybean oil for over 150 h on-stream [33]. Although dehydrated Zn–Al-LDHs exhibit superior basicity to $ZnAl_2O_4$ [29], they are disordered and hence hard to reproducibly prepare, and published routes are not alkali-free [33].

Activation of LDHs usually involves calcination–reconstruction protocols to partially exchange interlayer CO_3^{2-} with OH^- anions, thereby increasing basicity [34]. Liquid and vapour phase water reconstruction is known to influence the structure and performance of calcined Mg–Al-LDHs, however no such comparative studies exist for Zn–Al-LDHs for transesterification. Reconstruction of calcined Al^{3+} containing LDHs depends on the dissolution of M^{2+} cations into the amorphous AlO_x phase formed on calcination [35]. Zn–Al-LDHs are consequently more challenging to reconstruct than Mg–Al-LDH analogues [36] due to the different solubility products of $Zn(OH)_2$ and $Mg(OH)_2$ relative to $Al(OH)_3$ and concomitant energetics of ion dissolution–reprecipitation necessary to regenerate the LDH. Kooli et al. [37] demonstrated some success in regenerating lamellar structured materials following hydrothermal reconstruction of 300–400 °C calcined Zn–Al mixed oxides, although this has not been extended to alkali-free Zn–Al-LDHs or evaluated in catalytic applications.

Here the alkali-free synthesis of Zn–Al-LDHs is reported, and the impact of Zn:Al molar ratios and calcination–reconstruction protocols on corresponding basicity and catalytic activity explored. Hydrothermal reconstruction generates the most active catalysts for the transesterification of model C_4 – C_{18} triglycerides with methanol, with base site loadings and activity increasing with Zn content.

2. Results and Discussion

2.1. ZnAl-LDH Synthesis and Characterization

The successful synthesis of high surface area, alkali-free Zn–Al-LDHs with Zn:Al molar ratios spanning 1.6–3.3 was evidenced by powder XRD, elemental analysis, N_2 porosimetry, and SEM. Diffraction patterns characteristic of the hexagonal unit cell of LDHs [38] were observed in all cases (Figure 1), with sharp, intense reflections at $2\theta = 11^\circ, 23^\circ, 35^\circ, 39^\circ, 47^\circ, 60^\circ,$ and 62° corresponding to

(003), (006), (009), (102), (105), (108), (110), and (113) planes, respectively [29,39], with corresponding unit cell parameters of $a = 0.307 \pm 0.002$ nm and $c = 2.26 \pm 0.02$ nm in agreement with literature values for Zn–Al-LDH [37]. Zn:Al ratios determined by XRF fell within the typical range for LDHs, and systematically increased with nitrate precursor concentration (Table 1). The maximum Zn:Al ratio of 3.3 was lower than the nominal value of 4 expected from the synthesis, which may reflect a limit on the Zn^{2+} incorporation at pH 10 [40,41]. BET surface areas for as-synthesised materials spanned $43\text{--}73 \pm 5$ $\text{m}^2\cdot\text{g}^{-1}$, consistent with their similar crystallite sizes of $13\text{--}18 \pm 2$ nm determined from a Scherrer analysis; there is no systematic relationship between Zn:Al ratio and textural properties. SEM shows the $\text{Zn}_{1.6}\text{--Al-LDH}$ comprised small, stacked hexagonal platelets typical of ZnAl-LDHs (Figure 2); the platelet size increased with Zn:Al ratio, confirming with XRD that ordered, crystalline materials were obtained across the composition range.

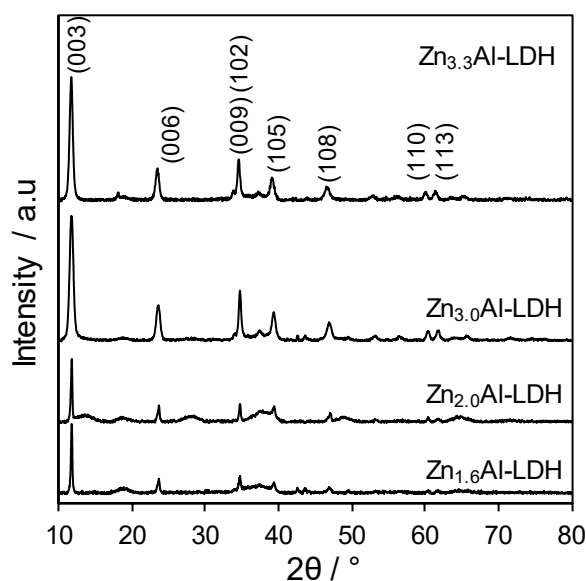


Figure 1. Powder XRD patterns of parent Zn–Al-LDHs synthesised via an alkali-free route.

Thermal analysis of the $\text{Zn}_{3.3}\text{--Al-LDH}$ material was subsequently employed to determine the optimum calcination temperature required to fully remove interlayer carbonate (Figure S1). Two weight losses were observed at 150 °C and 290 °C, coincident with H_2O and simultaneous $\text{H}_2\text{O}/\text{CO}_2$ evolution respectively, and hence are assigned to dehydration and hydroxycarbonate decomposition steps. A 300 °C calcination was therefore selected as the optimum temperature to remove interlayer CO_3^{2-} from ZnAl-LDHs; XRD confirmed the loss of LDH reflections and a concomitant emergence of new reflections at $2\theta = 31.8^\circ, 36.3^\circ, 47.6^\circ, 56.8^\circ$ assigned to a hexagonal wurtzite ZnO phase (Figure S2).

Table 1. Physicochemical properties of as-synthesised $\text{Zn}_x\text{Al-LDHs}$.

Nominal Zn:Al Atomic Ratio	Bulk Composition ^a		Experimental Zn:Al Atomic Ratio ^a	BET ^b Surface Area/ $\text{m}^2\cdot\text{g}^{-1}$	Crystallite ^c Size/nm
	Zn/wt%	Al/wt%			
1.5	30.9	8.0	1.6	43	18
2.0	32.3	6.7	2.0	63	15
3.0	33.5	4.6	3.0	73	18
4.0	44.2	5.5	3.3	65	13

^a XRF; ^b N_2 physisorption; ^c From XRD line broadening analysis using the Scherrer equation.

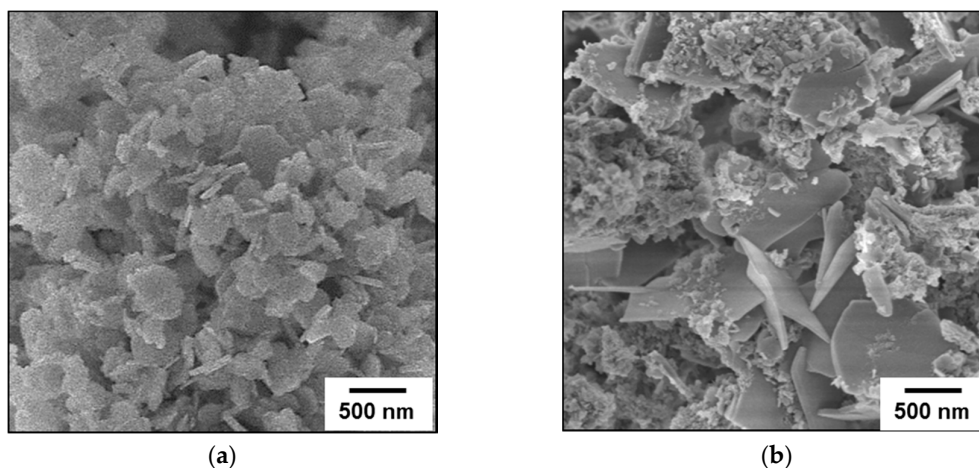


Figure 2. SEM images of alkali-free, as-synthesised Zn-Al-LDHs: (a) Zn_{1.6}-Al-LDH, and (b) Zn_{3.3}-Al-LDH.

Although ZnAl₂O₄ has a similar diffraction pattern to ZnO, the genesis of the former is discounted due to the high (>500 °C) calcination temperature required for its formation [42]. The ZnO reflections sharpen and intensify with LDH Zn content, indicating larger ZnO nanoparticles are extruded from the LDH platelets, whose initial sand rose structure is lost after 300 °C calcination, associated with the formation of agglomerates of 10–20 nm spherical particles (Figure S3).

Several literature protocols are reported for the reconstruction of LDHs from metal oxides arising from their calcination, including vapour [43] or liquid water [43,44], and hydrothermal processing [34], most notably for Mg-Al hydrotalcites. The effect of reconstruction protocol was therefore first investigated for the 300 °C calcined Zn_{3.3}-Al-LDH, which by analogy with Mg-Al hydrotalcites is anticipated to exhibit greatest basicity. Reconstruction was performed under water vapour wherein samples were cooled to room temperature under a flow of wet N₂ (steam), or in the solution phase wherein calcined samples were treated in deionised water at 25 °C (water), or 110 °C under autogeneous pressure (hydrothermal). XRD revealed that the degree of recovery of LDH reflections was greatest for a 110 °C hydrothermal treatment (73%), compared to steam (64%) or liquid water (25 °C) treatments (Figure 3).

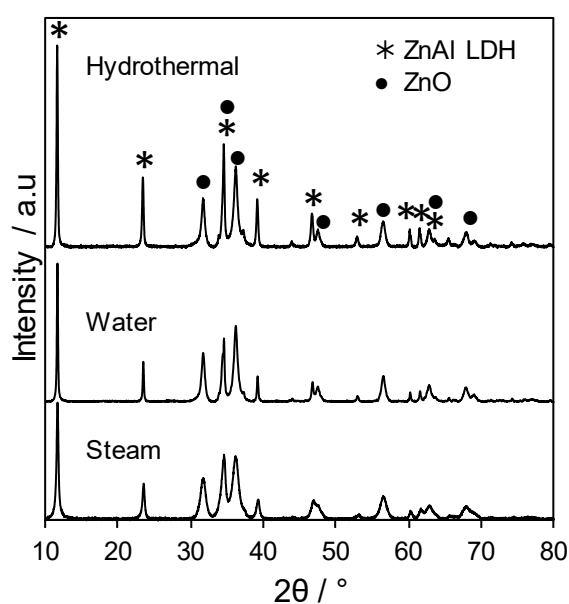


Figure 3. Powder XRD patterns of alkali-free Zn_{3.3}-Al-LDH following 300 °C calcination and subsequent reconstruction by steam, 25 °C water, or 110 °C hydrothermal treatments.

Larger (hexagonally-oriented) LDH crystallites were also obtained following hydrothermal treatment, consistent with more extensive recrystallisation (Figure 4); similar increased crystallinity is reported following hydrothermal aging of as-precipitated Zn–Al LDHs [40]. Water and steam treated materials retained significant fused spherical particles formed during calcination (Figure S3). Hydrothermal reconstruction also resulted in the highest surface area and base site loading compared to steam and water (Table 2), although CO₂ temperature-programmed desorption revealed little difference between the base strengths for each treatment (Figure S4).

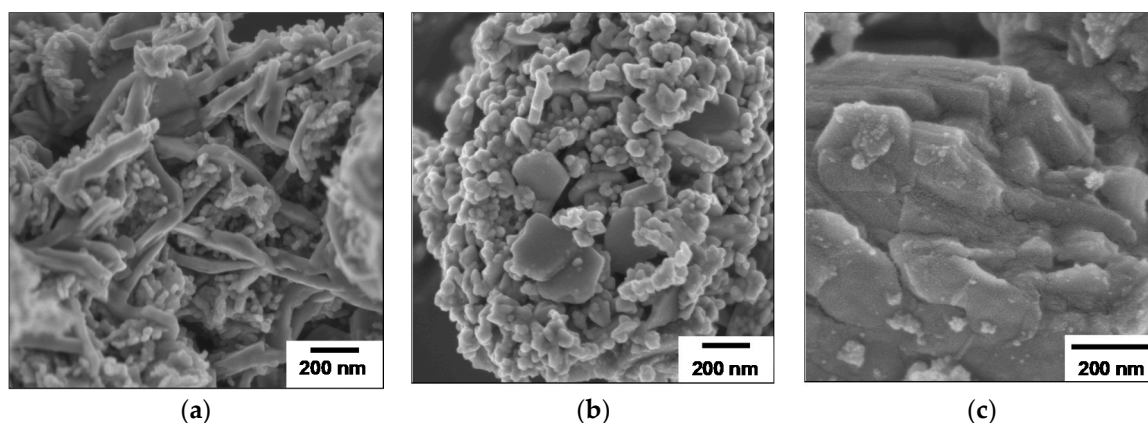


Figure 4. SEM images of alkali-free Zn_{3.3}–Al-LDHs following 300 °C calcination and subsequent reconstruction by (a) steam, (b) 25 °C water, and (c) 110 °C hydrothermal treatments.

Table 2. Physicochemical properties of 300 °C calcined Zn_{3.3}–Al-LDH materials following reconstruction via steam, 25 °C water or 110 °C hydrothermal treatments.

Reconstruction Protocol	LDH Crystallite Size ^a /nm	%Zn–Al-LDH ^b	BET Surface Area ^c /m ² ·g ^{−1}	Base Site Loading ^d	
				molecules·g ^{−1}	mmol·g ^{−1}
None	-	0	41	1.4 × 10 ¹⁹	0.023
Steam	15	64	81	2.4 × 10 ¹⁹	0.041
Water	25	64	87	2.6 × 10 ¹⁹	0.044
Hydrothermal	27	73	53	6.0 × 10 ¹⁹	0.10

^a From XRD line broadening analysis using the Scherrer equation; ^b From relative intensity of d(003) of LDH 2θ = 11.6° and d(101) of ZnO at 2θ = 36°; ^c N₂ physisorption; ^d CO₂ pulse chemisorption.

Hydrothermal activation was subsequently extended to the other 300 °C calcined ZnAl-LDHs (Figure S5), for which the extent of recovery of the LDH phase and corresponding LDH crystallite size increase with Zn content. Zn₄Al₂(OH)₁₀(CO₃)·xH₂O is reportedly the most stable LDH composition formed by hydrothermal aging of as-synthesised Zn_x–Al-LDHs, regardless of the initial composition [36,40], which might suggest complete reconstruction would be favoured by Zn–Al-LDHs with Zn:Al ratios ≤ 2:1. However in the present case, the efficiency of reconstruction from a calcined Zn–Al-LDH increases with Zn:Al ratio (Figure S5), suggesting that reconstruction it is not limited by the initial composition but rather by competing ZnO/ZnOH crystallisation. The basicity of the hydrothermally reconstructed LDHs linearly increased from 0.05 mmol·g^{−1} for Zn_{1.6}Al-LDH to 0.1 mmol·g^{−1} for Zn_{3.3}Al-LDH (Table S1), evidencing their tunable base properties.

2.2. Catalytic Activity

The influence of activation protocol on the catalytic performance of Zn_{3.3}–Al-LDH was subsequently evaluated for the transesterification of tributyrin with methanol (Figure S6). hydrothermal activation afforded significantly enhanced conversion than steam or water protocols (Figure 5). Turnover frequencies (TOFs) mirrored the trends in conversion. Since base strength was independent of activation protocol (Figure S4), the latter observation suggests that hydrothermal

activation improves the accessibility of base sites. TOFs of 180–290 h⁻¹ are consistent with literature values for solid base catalysed tributyrin transesterification (329 h⁻¹ for Mg₂Al-LDH [26,45], 220 h⁻¹ for Nano-MgO [46], and 100 h⁻¹ for Mg-ZrO₂ [47]). Tributyrin conversion increases with Zn:Al ratio across the hydrothermally activated Zn–Al-LDH family, reflecting the increased base site loading (Figure S7). TOFs were approximately independent of Zn:Al ratio, indicative of a common active site, although the Zn_{3.3}–Al-LDH appeared less susceptible towards deactivation (Figure S7). The Zn_{3.3}–Al-LDH catalyst stability was investigated by hot-filtration which confirmed the heterogenous nature of the catalyst (Figure S8).

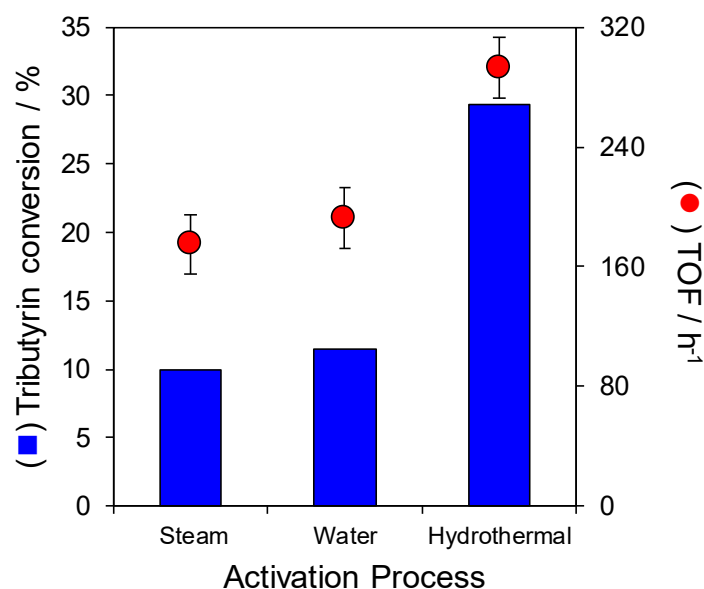


Figure 5. Effect of reconstruction protocol on tributyrin transesterification over Zn_{3.3}–Al-LDH. Reaction conditions: 65 °C, 6 h, 10 mmol tributyrin, 300 mmol methanol (TAG:alcohol molar ratio 1:30), 2.5 mmol dihexyl ether internal standard, 100 mg catalyst.

The most active Zn_{3.3}–Al-LDH catalyst was selected for the transesterification of longer chain C₈–C₁₈ TAGs (Figure S9 and Figure 6), for which 20 wt% 1-butanol was added to aid solubility, and the reaction temperature raised to 110 °C to compensate for the lower activity of bulky TAGs). As a control, transesterification of the C₄ TAG was also performed at 110 °C in the presence of butanol, revealing a 73% decrease in TOF, despite the increased reaction temperature, which may reflect competitive adsorption between less reactive but more strongly chemisorbed butoxide species [48] and methanol. Zn_{3.3}–Al-LDH was active for transesterification of all TAGs, however conversions and TOFs fell from 20 to 9% and 78 to 33 h⁻¹ respectively with increasing fatty acid chain length, possibly reflecting poorer base site accessibility for the bulkier TAGs. FAME selectivities after 24 h reaction exceeded 96% for C₄–C₈ TAGs, decreasing to 70–77% for the C₁₂ and C₁₈ TAGs (Table S2), suggesting that re-adsorption of longer chain DAG and MAG reactively-formed intermediates may also be hindered relative to shorter chain analogues.

Table S3 summarises the activity of representative solid base catalysts employed for the transesterification C₄–C₁₈ triglycerides and plant oils. The Zn_{3.3}–Al-LDH performance is comparable to that of Mg₂–Al-LDH catalysts [26] for tributyrin transesterification (290 versus 329 h⁻¹), and superior for triolein (33 versus 10.8 h⁻¹). Benchmarking against literature Zn–Al-LDH catalysts [31] is hindered by their higher reaction temperature (200 °C) and alkali precipitation synthesis route, which gives rise to homogenous contributions to measured catalytic activity [24]. The most promising report of Zn–Al-LDH is for soybean oil transesterification at 140 °C, wherein 76% conversion was observed under continuous flow at a (very low) weight hourly space velocity of 1 h⁻¹ [33]. In comparison, Zn_{3.3}–Al-LDH delivers a mass normalized productivity of 2.9 h⁻¹ at 110 °C for triolein

transesterification under batch conditions. Alkali-free, hydrothermally activated Zn–Al-LDHs are thus promising materials for the development of heterogeneously catalysed transesterification processes.

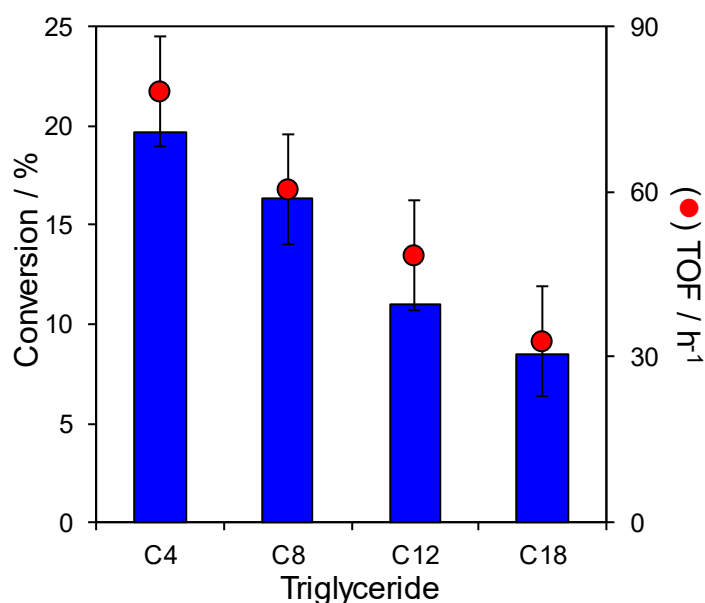


Figure 6. Activity of hydrothermally activated Zn_{3.3}-Al-LDH in transesterification of C₄-C₁₈ triglycerides with methanol at 110 °C. Conditions: 300 mmol MeOH, 10 mmol TAG, 2.5 mmol dihexyl ether internal standard, 20 wt% butanol, 100 mg Catalyst.

3. Materials and Methods

3.1. Catalyst Synthesis

Alkali-free Zn–Al-LDHs were prepared by co-precipitation, using simultaneous dropwise addition (1 mL·min⁻¹) of an aqueous solution of 1.5 M [Zn(NO₃)₂·6H₂O] (Sigma-Aldrich, Dorset, UK, reagent grade, 98%) and 1.5 M [Al(NO₃)₃·9H₂O] (Sigma-Aldrich ACS reagent ≥ 98%) (relative volumes adjusted to achieve nominal Zn:Al molar ratios spanning 1.5–4:1 with a total volume of 100 cm³), to a 100 cm³ solution of 2 M (NH₄)₂CO₃ (Sigma-Aldrich ACS reagent ≥ 30% NH₃ basis) in a 500 mL Radleys Reactor Ready (Saffron Waldon, UK) jacketed stirred reactor. A constant pH 10 was maintained throughout by this room temperature synthesis by the dropwise addition of aqueous ammonia (Sigma-Aldrich ACS reagent 28.0–30.0% NH₃). The mixture was then aged at 65 °C overnight under stirring, and the resulting solid product recovered by filtration, then washed with water until the washings were pH neutral and dried at 80 °C. The resulting catalysts are denoted Zn_x-Al-LDH, where x is the actual Zn:Al atomic ratio from XRF.

Catalysts were activated by calcination under flowing O₂ (20 mL·min⁻¹) at 300 °C for 5 h, and then reconstructed by different rehydration methods: steam, liquid water, or hydrothermal water. Steam activation was performed on calcined samples by cooling to room temperature under a flow of wet N₂ flow (bubbled at 20 mL·min⁻¹ through a water-filled Dreschel bottle) for 48 h, and dried at 80 °C prior to storage in a vacuum dessicator. For liquid water or hydrothermal activation, calcined samples were cooled to room temperature under nitrogen, then placed in 50 mL deionised water in either a stirred flask to 25 °C (water), or a stirred Teflon lined autoclave (hydrothermal) heated to 110 °C under autogeneous pressure, for 12 h. Liquid water and hydrothermally reconstructed LDHs were centrifuged, washed and dried at 80 °C prior to use.

3.2. Catalyst Characterisation

Zn–Al-LDHs were characterised by a powder XRD recorded on a Bruker-AXS D8 ADVANCE diffractometer (Coventry, UK) operated at 40 kV and 40 mA using Cu K_α radiation between 10–80°.

Crystallite sizes were determined by application of the Scherrer equation. XPS was performed on a Kratos Axis HSi X-ray photoelectron spectrometer (Manchester, UK) fitted with a charge neutraliser and magnetic focusing lens employing Al K_{α} monochromated radiation at 90 W. Spectral fitting was performed using CasaXPS version 2.3.16, with binding energies referenced to the C 1s peak at 284.5 eV. N_2 porosimetry was undertaken on a Quantachrome Nova 4000 porosimeter (Hook, UK) on samples degassed at 120 °C for 3 h. Surface areas were calculated by the Brunauer-Emmet-Teller (BET) method from the desorption isotherm for $P/P_0 < 0.2$. Base site densities were determined by CO_2 temperature program desorption (CO_2 -TPD) using a Quantachrome ChemBET 3000 chemisorption analyser (Hook, UK). 50 mg of the catalyst was placed in a quartz cell, outgassed for 1 h under flowing He at 120 °C, cooled to 40 °C, and then titrated with 50 μ L CO_2 pulses at room temperature. CO_2 TPD were obtained by heating CO_2 saturated samples to 700 °C at 10 °C·min⁻¹. Thermogravimetric analysis (TGA) was performed on a Mettler Toledo TGA/DSC2 Star system (Leicester, UK) under flowing nitrogen during heating to 800 °C at 10 °C·min⁻¹. Scanning Electron Microscopy (SEM) was performed on a JEOL JSM-7000F microscope (fitted with EDX) (Welwyn Garden City, UK) using a 20 kV accelerating voltage.

3.3. Catalytic Transesterification

Transesterification of tributyrin (Aldrich, 97%) with methanol (Fisher, 99.8%) was performed in a stirred, round-bottomed flask at 65 °C, using 100 mg or 50 mg of catalyst, 10 mmol of TAG, 300 mmol of methanol (TAG: alcohol mole ratio 1:30), and 2.5 mmol of dihexyl ether (Aldrich, 97%) as an internal standard. Comparison of hydrothermal activation protocols were performed at 65 °C using 100 mg catalyst owing to the low conversion of steam and liquid reconstructed materials, while 50 mg catalyst was employed when comparing the hydrothermal Zn_xAl family to ensure kinetics were measured free from any diffusion limitation.

Aliquots were periodically withdrawn from the reaction mixture and analysed by off-line GC after dilution with dichloromethane using a Varian 450-GC (Crawley, UK) fitted with a Phenomenex ZB-5HT Inferno column (15 m \times 0.32 mm i.d. and 0.1 μ m film thickness) capillary column. Due to poor miscibility of longer chain C_{8-18} TAGs (glyceryl trioctanoate, (Sigma, >90%), glyceryl trilaurate (Sigma, >90%) and glyceryl triolein (Alfa Aesar, 95%), 20 wt% of butanol (Sigma, >99.4%) was added to increase oil solubility in the reaction mixture, with transesterification performed at 110 °C in an ACE™ (Vineland, NJ, USA) pressure flask modified with a dip-tube to enable aliquots to be withdrawn. For consistency, the transesterification of the C_4 TAG was also performed with addition of butanol. Samples were diluted in dichloromethane, with analysis performed using a Varian 450-GC fitted with a temperature-programmed on-column injector and a Phenomenex ZB-1HT Inferno wide-bore column (15 m \times 0.53 mm and 0.1 μ m film thickness). Turnover Frequencies (TOFs) were calculated by normalising initial rates derived from the linear portion of reaction profiles (<20% conversion) during the first hour to the base site loadings obtained from CO_2 chemisorption.

Leaching studies were conducted using hot filtration and recycle tests to check the catalyst stability during tributyrin transesterification with methanol at 65 °C. For hot filtration tests, the catalyst was removed from the hot reaction after 3 h, followed by conversion and product formation for a further 24 h. Reusability of the recovered $Zn_{3.33}Al$ -LDH was also investigated following reactivation by calcination and hydrothermal reconstruction.

4. Conclusions

Zn - Al -LDHs with $Zn:Al$ molar ratios spanning 1.6–3.3 were successfully synthesised via an alkali-free route using NH_3OH and NH_3CO_3 . The influence of activation protocol on 300 °C calcined $Zn_{3.33}Al$ -LDH was explored, with hydrothermal reconstruction at 110 °C proving most effective for regenerating the parent LDH crystalline structure and maximizing the base site loading. All catalysts exhibited moderate strength base sites, attributed to $ZnOH$ in the LDH structure. Initial rates of tributyrin transesterification with methanol (and final conversion) were directly proportional to the Zn loading and hence base site density, suggesting that Zn - Al -LDHs possess a common base site. The

most active Zn_{3,3}-Al-LDH catalyst was stable towards leaching, and effective for the transesterification of C₄-C₁₈ triglycerides to FAMES, setting the scene for future evaluation against real oil feedstocks.

Supplementary Materials: The following are available online at <http://www.mdpi.com/2073-4344/8/12/667/s1>, Figure S1: (a) Mass loss and calorimetric measurements and (b) H₂O and CO₂ evolved followed by TG-MS during calcination of Zn_{3,3}-Al-LDH to 800 °C; Figure S2: Diffraction patterns of Zn_x-Al-LDH following calcination at 300 °C; Figure S3: SEM of Zn_{3,3}-Al-LDH following calcination at 300 °C; Figure S4: CO₂-TPD profiles of Zn_{3,3}-Al-LDH synthesised via steam, water or hydrothermal activation; Figure S5: (a) Diffraction patterns of Zn_x-Al-LDH (x-1.6-3.3), following hydrothermal activation; (b) % regeneration of LDH and crystallite size following hydrothermal activation; Figure S6: Effect of different activation protocols on activity of Zn_{3,3}-Al-LDH in tributyrin transesterification (a) tributyrin conversion, and (b) methyl butyrate yield; Figure S7: Effect of hydrothermally activated Zn_x-Al-LDH composition on tributyrin transesterification (a) tributyrin conversion, and (b) conversion after 24 h and TOF; Figure S8: Hot filtration leaching test for Zn_{3,3}-Al-LDH in the transesterification of tributyrin with methanol at 65 °C; Figure S9: Effect of TAG chain length on transesterification activity using hydrothermal Zn_{3,3}Al-LDH at 110 °C; Table S1: Physicochemical properties of hydrothermally activated Zn_x-Al-LDH materials; Table S2: Conversion and FAME selectivity following transesterification of different chain length TAGs over hydrothermally reconstructed Zn_{3,3}Al-LDH. Reaction conditions: 110 °C, 300 mmol MeOH, 10 mmol TAG, 2.5 mmol dihexyl ether internal standard, 20 wt% butanol, and 100 mg catalyst; Table S3: Conversion and TOF data from published literature of selected base catalysed transesterification of triglycerides.

Author Contributions: Conceptualization, A.F.L. and K.W.; Formal analysis, N.A.T., J.C.M., M.I., C.M.A.P., and K.W.; Investigation, N.A.T.; Methodology, N.A.T.; Supervision, A.F.L., and K.W.; Writing—original draft, N.A.T.; Writing—review & editing, A.F.L. and K.W.

Funding: This research was funded through a scholarship to NAT from the Malaysian Ministry of Higher Education (MOHE) and the University of Technology MARA (UiTM) Bestari Fund (600-IRMI/DANA5/3/BESTARI (050/2017)).

Conflicts of Interest: The authors declare no conflict of interest.

References

- Mardhiah, H.H.; Ong, H.C.; Masjuki, H.H.; Lim, S.; Lee, H.V. A review on latest developments and future prospects of heterogeneous catalyst in biodiesel production from non-edible oils. *Renew. Sustain. Energy Rev.* **2017**, *67*, 1225–1236. [CrossRef]
- Dickinson, S.; Mientus, M.; Frey, D.; Amini-Hajibashi, A.; Ozturk, S.; Shaikh, F.; Sengupta, D.; El-Halwagi, M.M. A review of biodiesel production from microalgae. *Clean Technol. Environ. Policy* **2017**, *19*, 637–668. [CrossRef]
- Ma, F.; Clements, L.D.; Hanna, M.A. Biodiesel Fuel from Animal Fat. Ancillary Studies on Transesterification of Beef Tallow. *Ind. Eng. Chem. Res.* **1998**, *37*, 3768–3771. [CrossRef]
- Mandolesi de Araújo, C.D.; de Andrade, C.C.; de Souza e Silva, E.; Dupas, F.A. Biodiesel production from used cooking oil: A review. *Renew. Sustain. Energy Rev.* **2013**, *27*, 445–452. [CrossRef]
- Knothe, G. Biodiesel: Current Trends and Properties. *Top. Catal.* **2010**, *53*, 714–720. [CrossRef]
- Mishra, V.K.; Goswami, R. A review of production, properties and advantages of biodiesel. *Biofuels* **2018**, *9*, 273–289. [CrossRef]
- Hajjari, M.; Tabatabaei, M.; Aghbashlo, M.; Ghanavati, H. A review on the prospects of sustainable biodiesel production: A global scenario with an emphasis on waste-oil biodiesel utilization. *Renew. Sustain. Energy Rev.* **2017**, *72*, 445–464. [CrossRef]
- Narasimharao, K.; Lee, A.; Wilson, K. Catalysts in Production of Biodiesel: A Review. *J. Biobased Mater. Bioenergy* **2007**, *1*, 19–30. [CrossRef]
- Luque, R.; Lovett, J.C.; Datta, B.; Clancy, J.; Campelo, J.M.; Romero, A.A. Biodiesel as feasible petrol fuel replacement: A multidisciplinary overview. *Energy Environ. Sci.* **2010**, *3*, 1706–1721. [CrossRef]
- Climent, M.J.; Corma, A.; Iborra, S.; Velty, A. Activated hydrotalcites as catalysts for the synthesis of chalcones of pharmaceutical interest. *J. Catal.* **2004**, *221*, 474–482. [CrossRef]
- Ono, Y.; Baba, T. Selective reactions over solid base catalysts. *Catal. Today* **1997**, *38*, 321–337. [CrossRef]
- Dacquín, J.-P.; Lee, A.F.; Wilson, K. Chapter 16 Heterogeneous Catalysts for Biodiesel Production. In *Thermochemical Conversion of Biomass to Liquid Fuels and Chemicals*; The Royal Society of Chemistry: London, UK, 2010; pp. 416–434.
- Wilson, K.; Lee, A.F. Rational design of heterogeneous catalysts for biodiesel synthesis. *Catal. Sci. Technol.* **2012**, *2*, 884. [CrossRef]

14. Ramachandran, K.; Suganya, T.; Nagendra Gandhi, N.; Renganathan, S. Recent developments for biodiesel production by ultrasonic assist transesterification using different heterogeneous catalyst: A review. *Renew. Sustain. Energy Rev.* **2013**, *22*, 410–418. [[CrossRef](#)]
15. Eze, V.C.; Phan, A.N.; Pirez, C.; Harvey, A.P.; Lee, A.F.; Wilson, K. Heterogeneous catalysis in an oscillatory baffled flow reactor. *Catal. Sci. Technol.* **2013**, *3*, 2373–2379. [[CrossRef](#)]
16. Wang, Q.; O'Hare, D. Recent Advances in the Synthesis and Application of Layered Double Hydroxide (LDH) Nanosheets. *Chem. Rev.* **2012**, *112*, 4124–4155. [[CrossRef](#)] [[PubMed](#)]
17. Cavani, F.; Trifirò, F.; Vaccari, A. Hydrotalcite-type anionic clays: Preparation, properties and applications. *Catal. Today* **1991**, *11*, 173–301. [[CrossRef](#)]
18. Helwani, Z.; Othman, M.R.; Aziz, N.; Kim, J.; Fernando, W.J.N. Solid heterogeneous catalysts for transesterification of triglycerides with methanol: A review. *Appl. Catal. A Gen.* **2009**, *363*, 1–10. [[CrossRef](#)]
19. Othman, M.R.; Helwani, Z.; Martunus; Fernando, W.J.N. Synthetic hydrotalcites from different routes and their application as catalysts and gas adsorbents: A review. *Appl. Organomet. Chem.* **2009**, *23*, 335–346. [[CrossRef](#)]
20. Yan, K.; Liu, Y.; Lu, Y.; Chai, J.; Sun, L. Catalytic application of layered double hydroxide-derived catalysts for the conversion of biomass-derived molecules. *Catal. Sci. Technol.* **2017**, *7*, 1622–1645. [[CrossRef](#)]
21. Fan, G.; Li, F.; Evans, D.G.; Duan, X. Catalytic applications of layered double hydroxides: Recent advances and perspectives. *Chem. Soc. Rev.* **2014**, *43*, 7040–7066. [[CrossRef](#)] [[PubMed](#)]
22. Costantino, U.; Marmottini, F.; Nocchetti, M.; Vivani, R. New synthetic routes to hydrotalcite-like compounds—Characterisation and properties of the obtained materials. *Eur. J. Inorg. Chem.* **1998**, 1439–1446. [[CrossRef](#)]
23. Fraile, J.M.; García, N.; Mayoral, J.A.; Pires, E.; Roldán, L. The influence of alkaline metals on the strong basicity of Mg–Al mixed oxides: The case of transesterification reactions. *Appl. Catal. A Gen.* **2009**, *364*, 87–94. [[CrossRef](#)]
24. Cross, H.E.; Brown, D.R. Entrained sodium in mixed metal oxide catalysts derived from layered double hydroxides. *Catal. Commun.* **2010**, *12*, 243–245. [[CrossRef](#)]
25. Cantrell, D.G.; Gillie, L.J.; Lee, A.F.; Wilson, K. Structure-reactivity correlations in MgAl hydrotalcite catalysts for biodiesel synthesis. *Appl. Catal. A Gen.* **2005**, *287*, 183–190. [[CrossRef](#)]
26. Woodford, J.J.; Dacquin, J.-P.; Wilson, K.; Lee, A.F. Better by design: Nanoengineered macroporous hydrotalcites for enhanced catalytic biodiesel production. *Energy Environ. Sci.* **2012**, *5*, 6145–6150. [[CrossRef](#)]
27. Helwani, Z.; Aziz, N.; Kim, J.; Othman, M.R. Improving the yield of *Jatropha curcas*'s FAME through sol-gel derived meso-porous hydrotalcites. *Renew. Energy* **2016**, *86*, 68–74. [[CrossRef](#)]
28. Hibino, T.; Ohya, H. Synthesis of crystalline layered double hydroxides: Precipitation by using urea hydrolysis and subsequent hydrothermal reactions in aqueous solutions. *Appl. Clay Sci.* **2009**, *45*, 123–132. [[CrossRef](#)]
29. Montanari, T.; Sisani, M.; Nocchetti, M.; Vivani, R.; Delgado, M.C.H.; Ramis, G.; Busca, G.; Costantino, U. Zinc–aluminum hydrotalcites as precursors of basic catalysts: Preparation, characterization and study of the activation of methanol. *Catal. Today* **2010**, *152*, 104–109. [[CrossRef](#)]
30. Quirino, M.R.; Oliveira, M.J.C.; Keyson, D.; Lucena, G.L.; Oliveira, J.B.L.; Gama, L. Synthesis of zinc aluminate with high surface area by microwave hydrothermal method applied in the transesterification of soybean oil (biodiesel). *Mater. Res. Bull.* **2016**, *74*, 124–128. [[CrossRef](#)]
31. Jiang, W.; Lu, H.-F.; Qi, T.; Yan, S.-L.; Liang, B. Preparation, application, and optimization of Zn/Al complex oxides for biodiesel production under sub-critical conditions. *Biotechnol. Adv.* **2010**, *28*, 620–627. [[CrossRef](#)] [[PubMed](#)]
32. Stern, R.H.G.; Rouxel, J.-J.; Leporq, S. Process for the Production of Esters from Vegetable oils or Animal Oils Alcohols. U.S. Patent 5,908,946, 1 June 1999.
33. Liu, Q.; Wang, B.; Wang, C.; Tian, Z.; Qu, W.; Ma, H.; Xu, R. Basicities and transesterification activities of Zn–Al hydrotalcites-derived solid bases. *Green Chem.* **2014**, *16*, 2604–2613. [[CrossRef](#)]
34. Abelló, S.; Medina, F.; Tichit, D.; Pérez-Ramírez, J.; Groen, J.C.; Sueiras, J.E.; Salagre, P.; Cesteros, Y. Aldol Condensations Over Reconstructed Mg–Al Hydrotalcites: Structure–Activity Relationships Related to the Rehydration Method. *Chem. A Eur. J.* **2004**, *11*, 728–739. [[CrossRef](#)] [[PubMed](#)]

35. Li, W.; Livi, K.J.T.; Xu, W.; Siebecker, M.G.; Wang, Y.; Phillips, B.L.; Sparks, D.L. Formation of Crystalline Zn–Al Layered Double Hydroxide Precipitates on γ -Alumina: The Role of Mineral Dissolution. *Environ. Sci. Technol.* **2012**, *46*, 11670–11677. [[CrossRef](#)] [[PubMed](#)]
36. Prikhod'ko, R.V.; Sychev, M.V.; Astrelin, I.M.; Erdmann, K.; Mangel, A.; van Santen, R.A. Synthesis and Structural Transformations of Hydrotalcite-like Materials Mg–Al and Zn–Al. *Russ. J. Appl. Chem.* **2001**, *74*, 1621–1626. [[CrossRef](#)]
37. Kooli, F.; Depege, C.; Ennaqadi, A.; de Roy, A.; Besse, J.P. Rehydration of Zn–Al layered double hydroxides. *Clays Clay Miner.* **1997**, *45*, 92–98. [[CrossRef](#)]
38. Pachayappan, L.; Nagendran, S.; Kamath, P.V. Reappraisal of Polytypism in Layered Double Hydroxides: Consequences of Cation Ordering in the Metal Hydroxide Layer. *Cryst. Growth Des.* **2017**, *17*, 2536–2543. [[CrossRef](#)]
39. Millange, F.; Walton, R.I.; O'Hare, D. Time-resolved in situ X-ray diffraction study of the liquid-phase reconstruction of Mg–Al–carbonate hydrotalcite-like compounds. *J. Mater. Chem.* **2000**, *10*, 1713–1720. [[CrossRef](#)]
40. Klopogge, J.T.; Hickey, L.; Frost, R.L. The effects of synthesis pH and hydrothermal treatment on the formation of zinc aluminum hydrotalcites. *J. Solid State Chem.* **2004**, *177*, 4047–4057. [[CrossRef](#)]
41. Bocclair, J.W.; Braterman, P.S. Layered Double Hydroxide Stability. 1. Relative Stabilities of Layered Double Hydroxides and Their Simple Counterparts. *Chem. Mater.* **1999**, *11*, 298–302. [[CrossRef](#)] [[PubMed](#)]
42. Zhao, X.; Zhang, F.; Xu, S.; Evans, D.G.; Duan, X. From Layered Double Hydroxides to ZnO-based Mixed Metal Oxides by Thermal Decomposition: Transformation Mechanism and UV-Blocking Properties of the Product. *Chem. Mater.* **2010**, *22*, 3933–3942. [[CrossRef](#)]
43. Tichit, D.; Bennani, M.N.; Figueras, F.; Tessier, R.; Kervennal, J. Aldol condensation of acetone over layered double hydroxides of the meixnerite type. *Appl. Clay Sci.* **1998**, *13*, 401–415. [[CrossRef](#)]
44. Abelló, S.; Medina, F.; Tichit, D.; Perez-Ramirez, J.; Cesteros, Y.; Salagre, P.; Sueiras, J. Nanoplatelet-based reconstructed hydrotalcites: Towards more efficient solid base catalysts in aldol condensations. *Chem. Commun.* **2005**, 1453–1455. [[CrossRef](#)] [[PubMed](#)]
45. Creasey, J.J.; Chieragato, A.; Manayil, J.C.; Parlett, C.M.A.; Wilson, K.; Lee, A.F. Alkali- and nitrate-free synthesis of highly active Mg–Al hydrotalcite-coated alumina for FAME production. *Catal. Sci. Technol.* **2014**, *4*, 861–870. [[CrossRef](#)]
46. Montero, J.M.; Brown, D.R.; Gai, P.L.; Lee, A.F.; Wilson, K. In situ studies of structure-reactivity relations in biodiesel synthesis over nanocrystalline MgO. *Chem. Eng. J.* **2010**, *161*, 332–339. [[CrossRef](#)]
47. Rabee, A.; Manayil, J.; Isaacs, M.; Parlett, C.; Durndell, L.; Zaki, M.; Lee, A.; Wilson, K. On the Impact of the Preparation Method on the Surface Basicity of Mg–Zr Mixed Oxide Catalysts for Tributyrin Transesterification. *Catalysts* **2018**, *8*, 228. [[CrossRef](#)]
48. Campbell, C.T.; Sellers, J.R.V. Enthalpies and Entropies of Adsorption on Well-Defined Oxide Surfaces: Experimental Measurements. *Chem. Rev.* **2013**, *113*, 4106–4135. [[CrossRef](#)] [[PubMed](#)]

